

# Fatigue strength of high-strength steel after shipyard production process of plasma cutting, grinding, and sandblasting

Ingrit Lillemäe-Avi<sup>1,2</sup> · Sami Liinalampi<sup>2</sup> · Eero Lehtimäki<sup>2</sup> · Heikki Remes<sup>2</sup> · Pauli Lehto<sup>2</sup> · Jani Romanoff<sup>2</sup> · Sören Ehlers<sup>3</sup> · Ari Niemelä<sup>1</sup>

Received: 4 September 2017 / Accepted: 7 August 2018 / Published online: 14 September 2018  
© International Institute of Welding 2018

## Abstract

This paper investigates experimentally the fatigue strength of high-strength steel, which has undergone the normal shipyard production process of plasma cutting, grinding, and sandblasting. The study includes steels with the yield strength of 355 and 690 MPa. The tested specimens are of dog-bone shape and represent the large-scale situation of a cruise ship balcony opening corner, loaded in shear or tension. The influence of surface roughness, internal inclusions, hardness, and residual stress on the fatigue strength are studied and discussed. Compared to the design curve as well as to the untreated surfaces, the results show significantly improved fatigue strength under constant amplitude loading at a load ratio of  $R = 0.1$ . However, very flat or even rising slope of the S-N curve indicates variations in the material and surface quality as well as in the residual stress. Surprisingly, internal defects even up to 100 µm in size did not decrease the fatigue strength.

**Keywords** Fatigue strength · High-strength steel · Surface integrity · Inclusions · Hardness · Residual stress · Large-scale testing · Ship structure

## 1 Introduction

Next-generation large steel structures should have excellent energy efficiency and load carrying capacity—goals for which new lightweight solutions are needed. Better utilization of high-strength steels together with the advanced production technology has high potential for weight reduction. However, due to lack of knowledge about the fatigue resistance, current classification rules do not yet allow realizing the full potential of high-strength steels in lighter designs [1–3].

Traditional production methods applicable for mild steel induce initial crack-like defects into the material. As higher-strength steel is more sensitive to these initial defects [4], a phenomenon called notch sensitivity, the increased fatigue strength is lost. By appropriate post-treatment of critical structural details such as welds and plate edges, the initial defects can be removed. In large structures such as passenger ships, the most fatigue critical structural details, in addition to welds, are the corners of openings in the load-carrying structural members; see Fig. 1.

Remes et al. [5] investigated the influence of surface integrity on the fatigue strength of high-strength steel used in large marine structures, e.g., the side shell with balcony openings. The investigation included full-scale specimens with the yield strength  $\sigma_y$  of 355, 460, and 690 MPa. After plasma cutting, the plate edges were treated with methods suitable for shipyard production, i.e., grinding and grinding followed by sandblasting. The plasma cutting introduced a heat-affected layer with very high hardness, which was not influenced by grinding or sandblasting. Nevertheless, the results showed significant yield strength-dependent increase in the fatigue strength for treated specimens due to better surface roughness and beneficial compressive residual stress. Similar increase in fatigue strength after

---

Recommended for publication by Commission XIII - Fatigue of Welded Components and Structures

✉ Ingrit Lillemäe-Avi  
Ingrit.lillemae@gmail.com

<sup>1</sup> Meyer Turku Oy, Telakkakatu 1, 20240 Turku, Finland

<sup>2</sup> School of Engineering, Department of Mechanical Engineering, Aalto University, P.O. BOX 13400, FI-00076 Aalto, Finland

<sup>3</sup> Hamburg University of Technology, Am Schwarzenberg-Campus 4, 21073 Hamburg, Germany

**Fig. 1** Example of a fatigue critical opening corner, modified from [5]

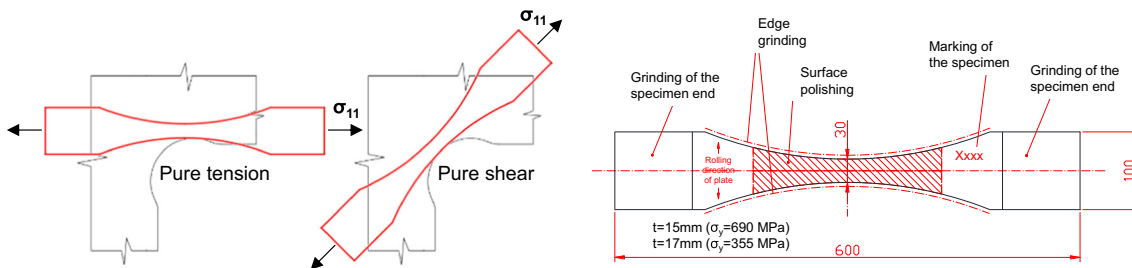
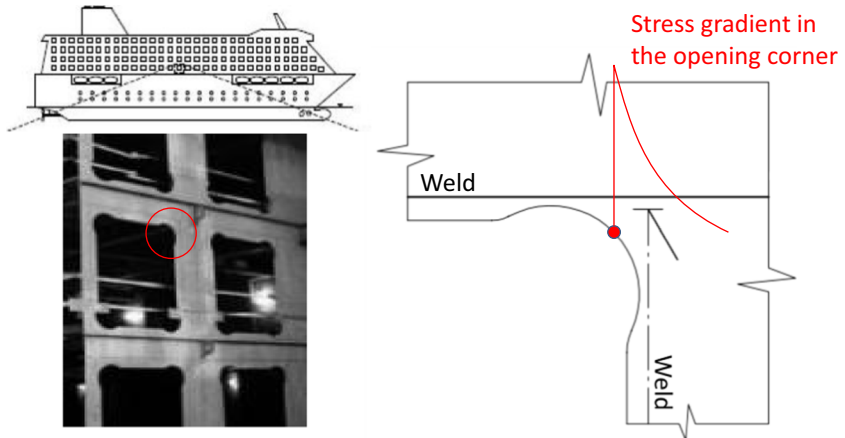


**Fig. 2** Large-scale dog-bone specimen simulating the first principal stress at the opening corner under the shear and tension loading

treatment is visible in [6]. In addition, Sperle [7] and Laitinen et al. [8] showed that the higher fatigue strength can also be achieved without treatment if the cutting quality is good.

However, the number of repetitions in the previous tests was too limited to cover the manufacturing variations. In addition, the results were obtained in the finite life region with the load cycles to failure between  $10^5$  and  $10^6$ , with the run-out limit specified at two to five million. In reality, ship structures encounter up to  $10^8$  load cycles, if typical lifetime is assumed to be 25 years and majority of waves have a zero up-crossing period of 7–11 s; see e.g. [9]. Several researchers have reported fatigue failures after  $10^7$  cycles, and it has been often shown that in the range of  $10^6$ – $10^8$  the failure mechanism changes and the cracks start to initiate from the

subsurface defects such as inclusions and pores instead of material surface; see, e.g., [10–16]. The experimental results have shown that it is unsafe to assume infinite life after the specimen has lasted a certain number of cycles. As these studies utilized small-scale polished laboratory specimens, the question remains how the typical shipyard production process of plasma cutting followed by grinding and sandblasting influences the fatigue strength of high-strength steel in very high cycle regions.

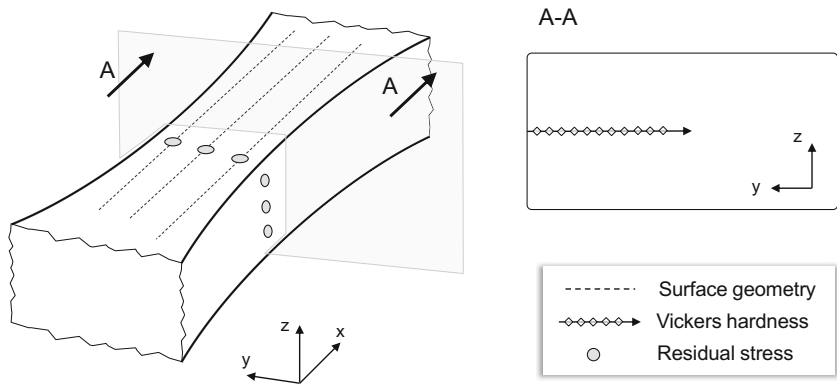
The goal of this study is to investigate the fatigue strength and failure mechanism of shipyard-processed high-strength steel in very high cycle fatigue ranges, i.e., more than two million load cycles. The influences of surface roughness, internal defects, hardness, and residual stress on the fatigue strength are studied and discussed.

**Table 1** Material properties

Material	Yield strength $R_{eH}$ (MPa)	Ultimate tensile strength $R_m$ (MPa)	Failure strain (%)
355 (AH36 hot rolled steel plates)	437	566	24
690 (NVE690 Q)	850	890	16

**Table 2** Chemical composition (%)

Material	C	Si	Mn	P	S	Al	Nb	V	Ti	Cu	Cr	Ni	Mo	B	N
355 (AH36)	0.14	0.44	1.38	0.007	0.002	0.033	0.042	0.007	0.004	0.05	0.06	0.06	0.009		
690 (NVE690)	0.16	0.21	1.39	0.011	0.001	0.047	0.015	0.018	0.007	0.01	0.25	0.06	0.502	0.001	0.002

**Fig. 3** Surface roughness, hardness, and residual stress measurement locations

## 2 Experiments

### 2.1 Specimens

The uniaxial fatigue test specimen used in this study was similar to previous investigation in [5] and is presented in Fig. 2. It represents the full-scale condition as the failure always occurs in the direction of maximum principal stress, while the exact location of failure within the corner changes depending on the ratio between the ship hull girder vertical bending moment and shear force. Specimens were 600 mm long and 30–100 mm wide. They were plasma cut from the 17-mm-thick plate with the nominal yield strength of 355 MPa and from the 15-mm-thick 690 MPa plate. The material properties are presented in Table 1 and chemical composition in Table 2. After plasma cutting, the plates were grinded or grinded and

sandblasted, which is normal shipyard practice before applying the paint.

### 2.2 Roughness measurements

The effect of post-cut treatment on the surface roughness was studied according to EN ISO 4288 [17] using contact stylus-type device Mitutoyo Surftest. From each series, two or three specimens were measured. For each measured specimen, the values along six lines were defined, three on top and three on bottom plate surface (see Fig. 3). The evaluation length of one line was 16 mm containing five sampling lengths of 3.2 mm. A Gaussian filter was applied. From the measured profiles, three parameters were determined: (1) arithmetical average height of the surface roughness  $R_a$ , (2) maximum peak to valley height  $R_{z\_max}$ , and (3) arithmetical average of maxi-

**Table 3** Fatigue test program

Specimen series	Test description	Load ratio	No. of specimens
690 grinded	CAL fatigue test	0.1	11
690 grinded and sandblasted	CAL fatigue test	0.1	14
355 grinded	CAL fatigue test	0.1	4
355 grinded and sandblasted	CAL fatigue test	0.1	10
690 grinded and sandblasted	WASH spectrum loading	0.5	1
		Total:	40



**Fig. 4** Specimen in the resonant testing machine of TUHH

mum peak to valley heights in five equidistant sampling lengths  $R_{z5}$ . The measurements were limited to plate surfaces because the previous study [5] did not reveal significant differences in roughness between plate surface and cut specimen edge.

### 2.3 Hardness measurements and microstructural analysis

The effect of plasma-cutting and post-treatment on the microstructure of cut edges were studied using macrosamples and Vickers hardness (HV0.3) measurements according to EN ISO 6507 [18]. Hardness testing was carried out with Buehler Micromet 2101 instrument. Prior to hardness measurements, the macrosamples were mounted in epoxy resin and grinded up to P2400 grit abrasive paper, followed by polishing with 3  $\mu\text{m}$  and 1  $\mu\text{m}$  diamond paste. The samples were etched with a 2% Nital solution to reveal the microstructure. The hardness measurement points are shown in Fig. 3. After the fatigue testing, fracture surfaces were photographed with a microscope to categorize the crack initiation locations. Selected samples were examined also using the Zeiss Ultra 55 field emission scanning electron microscope.

### 2.4 Residual stress measurements

The effect of post-cut treatment on the residual stress was measured using X-ray diffraction with Stresstech X3000

device in accordance with EN ISO 15305:2007 [19]. The measurement points were in the middle of the specimen, on both plate surfaces and cut edges (see Fig. 3). The circular collimator diameter was 3 mm, radiation source was Cr-K $\alpha$  (30 kV, 6.7 mA) and exposure time 5 s; 6/6 psi tilts were used. For stress evaluation, Young's modulus  $E$  of 211 GPa and Poisson ratio  $\nu$  of 0.3 were used. Measurements were carried out in initial condition, i.e., as delivered from the shipyard. In total, two grinded and six sandblasted specimens were measured.

### 2.5 Fatigue tests

The test program consisted of 40 dog-bone specimens as summarized in Table 3. Tests included constant amplitude (CAL) experiments with a load ratio of  $R = 0.1$ . In addition, one specimen was tested under variable amplitude WASH spectrum loading (VAL) (see [20]). Tests were carried out in Hamburg University of Technology (TUHH) in Germany, using a resonant test rig with the testing frequency of approximately 32 Hz (see Fig. 4).

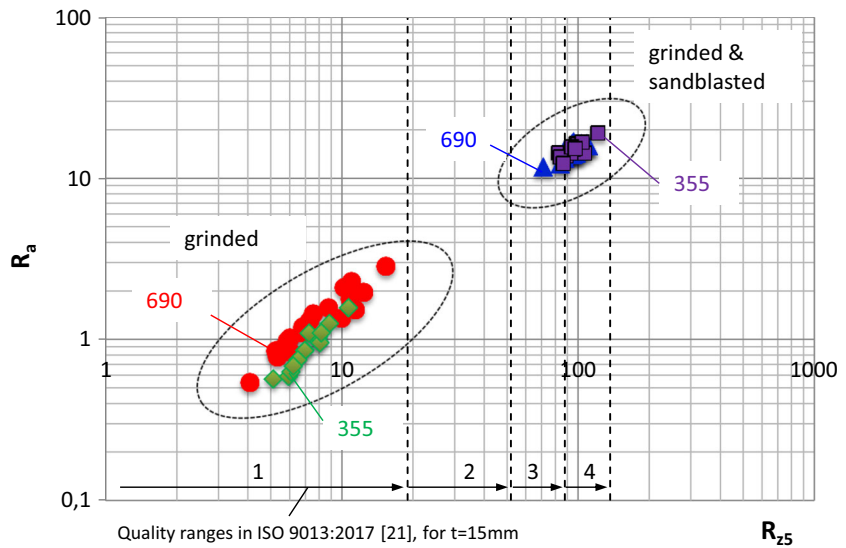
## 3 Results

### 3.1 Surface roughness

Surface roughness parameters are summarized in Table 4 and plotted in terms of average ( $R_a$ ) and average of maximum peak-to-valley heights in five equidistant sampling lengths ( $R_{z5}$ ) in Fig. 5. Examples of surface profiles for 690 steel together with the definition of  $R_{z5}$  are presented in Fig. 6. In the case of grinded and sandblasted surface, the roughness  $R_a$  is about 15  $\mu\text{m}$  for both 355 and 690 steels. For grinded surface, the average roughness  $R_a$  is around 1  $\mu\text{m}$  being slightly higher for 690 steel than that of 355 steel. The  $R_{z5}$  values are approximately 10  $\mu\text{m}$  for grinded surfaces and 100  $\mu\text{m}$  for grinded and sandblasted specimens. The values and variation both are similar, but slightly larger compared to previous results reported in [5, 7]. According to ISO:9013 [21], the grinded specimens belong to the first and sandblasted to the

**Table 4** Summary of surface roughness: minimum ... mean ... maximum (standard deviation)

Series	$R_a$ ( $\mu\text{m}$ )	$R_{z\_max}$ ( $\mu\text{m}$ )	$R_{z5}$ {ISO 9013 quality range} ( $\mu\text{m}$ )
690 grinded	0.5 ... 1.3 ... 2.8 (0.6)	5.7 ... 12 ... 27 (5.3)	4.1 ... 8 ... 15 (3.1) {1}
690 grinded and sandblasted	12 ... 15 ... 17 (1.5)	102 ... 125 ... 158 (16.8)	71 ... 96 ... 110 (9.8) {3-4}
355 grinded	0.6 ... 0.9 ... 1.6 (0.3)	7.1 ... 10.8 ... 18.2 (3.2)	5.1 ... 7.3 ... 11 (1.5) {1}
355 grinded and sandblasted	12 ... 15 ... 19 (1.8)	98 ... 131 ... 181 (25.7)	83 ... 96...121 (10.9) {3-4}

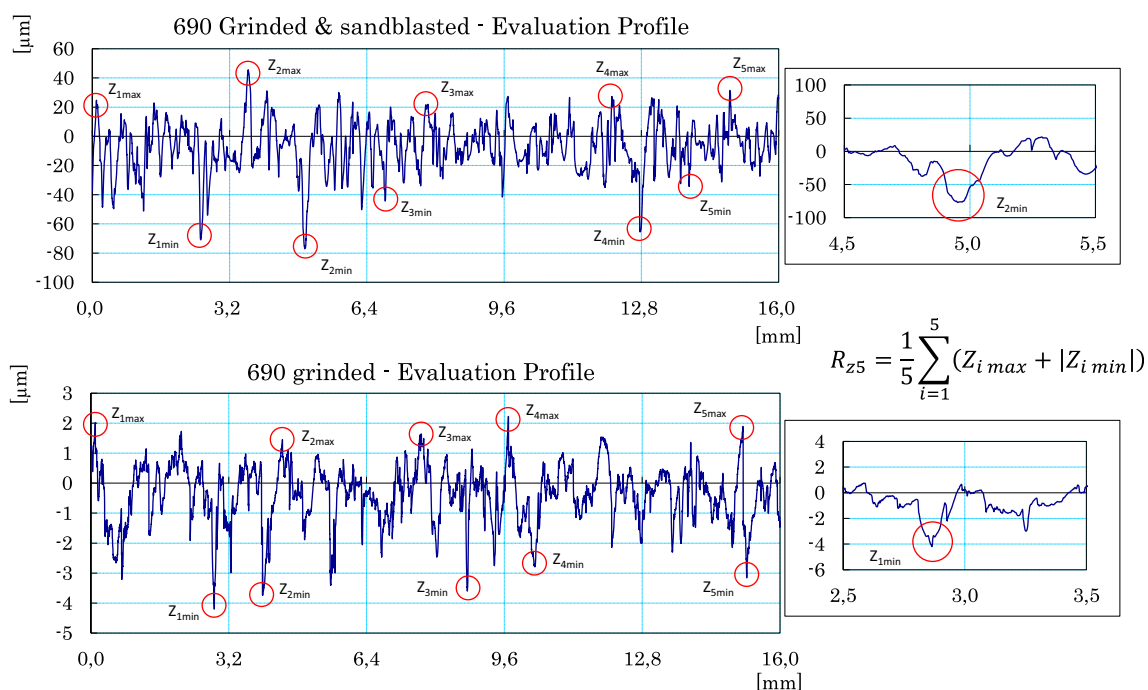
**Fig. 5** Surface roughness

third or fourth, i.e., the worst quality class (see Fig. 5). Even though sandblasting results in about 10 times larger surface roughness, the profile is also smoother. Grinded specimens have sharper peaks and valleys, which can act as initial cracks (see Fig. 6).

### 3.2 Microstructure and hardness

Hardness of the plasma cut edge is plotted over the macrograph in Fig. 7 for 690 and in Fig. 8 for 355 steel. In both

cases, the hardness in the heat-affected zone (HAZ) after plasma cutting is approximately double the value in the base material (BM), i.e., 305 in BM and up to 551 HV0.3 in HAZ of 690 steel and 196 in BM and up to 404 HV0.3 in HAZ of 355 steel. The maximum hardness of the 355 plasma-cut edge is similar as previously presented in [22] and slightly lower compared to [5] (see Table 5). For 690 steel, the value is larger compared to [5, 22]. The depth of the hardened layer is about 250 µm for 690 steel and 350 µm for 355 steel, respectively. In addition, it can be observed that hardness gradient between

**Fig. 6** Examples of surface profiles for 690 grinded and sandblasted (upper) and 690 grinded steel (lower)

**Fig. 7** Microhardness for 690 plasma cut edge

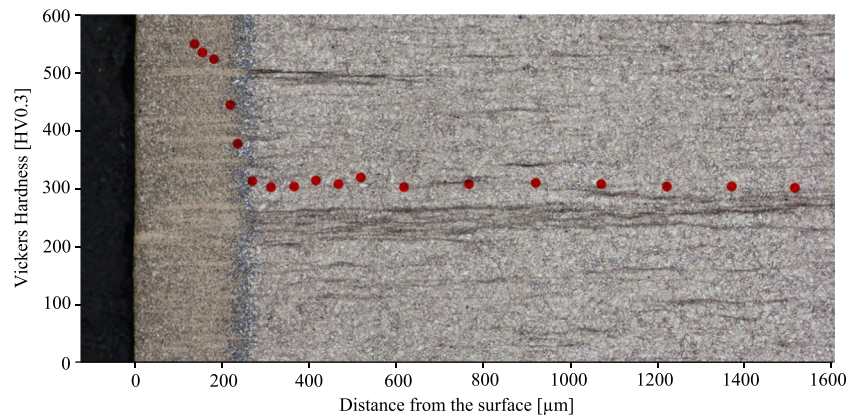
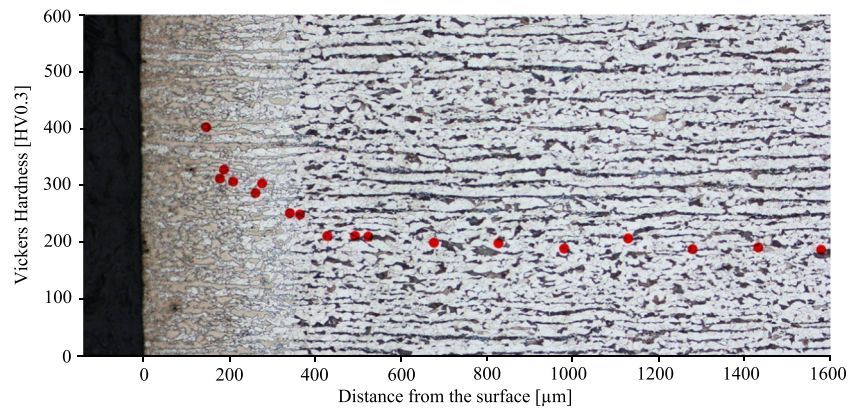


**Fig. 8** Microhardness for 355 plasma cut edge



the hardened layer and base material is steeper for 690 steel than for 355 steel, where a wide and smooth transition area is visible.

### 3.3 Residual stress

Residual stresses transverse to the loading direction are presented in Fig. 9. The measurements include two 690 grinded specimens and six 690 sandblasted specimens. Compressive residual stresses down to approximately  $-400$  MPa can be seen in the cut edge, both in the case of grinded as well as grinded and sandblasted specimens. In the plate surface, the residual stress down to  $-300$  MPa can be observed in grinded specimens, while sandblasted specimens have lower values as well as smaller variation. Based on these and previous results [5], it seems that sandblasting does not reduce residual stresses in the hardened cut edge, but does so in the plate surface. Compared to the previous study [5], the observed maximum values of compressive residual stresses transverse to the load direction are up to three times larger. This may be due to higher number of measurement points in the current investigation, which has highlighted the large variation within some specimens. Furthermore, the results are different from the

untreated plasma cut edges reported earlier, where the residual stresses were close to zero [5] or even slightly tensile [23].

## 3.4 Fatigue test results

### 3.4.1 Fatigue strength

Fatigue test results for all specimens tested with the stress ratio of  $R = 0.1$  are presented in Fig. 10 and summarized in Table 6. The table also includes the results for treated and untreated plasma cut edges from the previous studies. The figure includes the run-out specimens that are retested at higher load level, but these data points are not included in the statistical analysis;

**Table 5** Comparison of maximum hardness in plasma cut edge

	355	690
Current study	404 ( $t = 17$ mm)	551 ( $t = 15$ mm)
Remes et al. 2013 [5]	460 ( $t = 17$ mm)	510 ( $t = 15$ mm)
Lefebvre et al. 2015 [22]	412 ( $t = 15$ mm)	341 ( $t = 5$ mm)

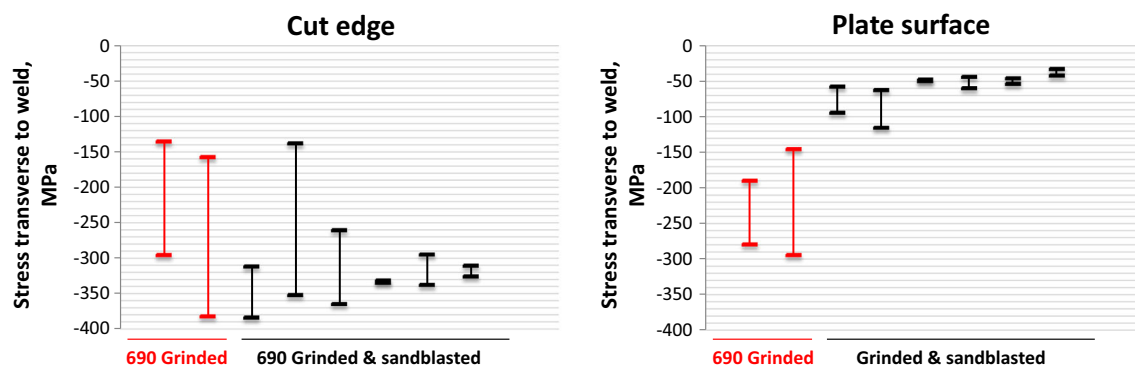


**Fig. 9** Residual stress on cut edge (left) and plate surface (right), variation between specimens as well as within each specimen shown

see more from Appendix. It can be seen that the slopes of the test data are quite flat or even rising with the number of cycles, and therefore, the statistical parameters of the S-N curve are calculated using the same slope value of  $m = 15.4$  for all series to allow for a comparison between them (Table 6 and Fig. 10). Note that Fig. 10 also includes data points from the previous study [5], but these points are not included in the statistical analysis. Fatigue strength for 690 steel is significantly higher than that of 355 steel, but the difference in fatigue strength between grinded and sandblasted specimens is very small. For 690 grinded series, significant scatter can be observed (see Fig. 10 and Table 6).

Figure 10 includes two design curves, FAT160 with the negative inverse slope  $m = 4$  [3] and FAT235 with  $m = 4.7$  [24]. The higher FAT class is associated with steels having yield strength of 500 MPa or above, and average surface roughness of  $R_a \leq 3.2 \mu\text{m}$ , loaded in tension only with high mean stress. In addition, Lefebvre et al. 2015 [22] proposed FAT245 and  $m = 5$  for steels S690/S700 with the surface roughness of  $R_z < 100 \mu\text{m}$ . All test results of current study for 690 and 355 steel are above of these reference curves, even

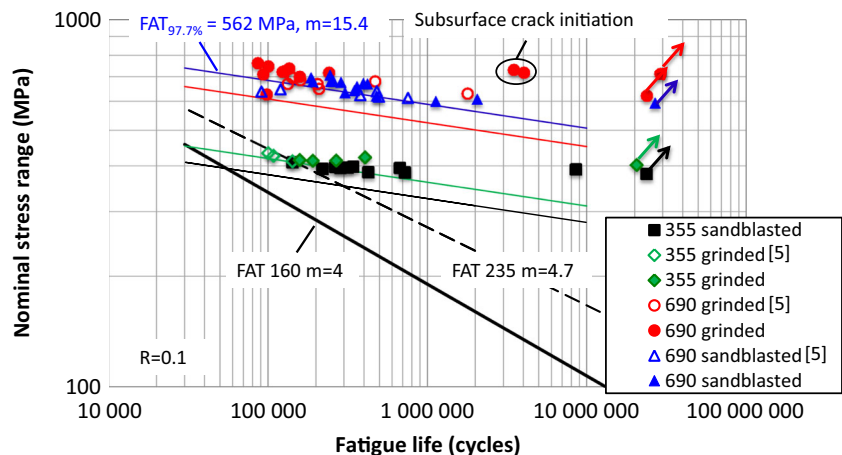
though  $R_a$  and  $R_z$  values exceed these specified limits in case of sandblasted surfaces.

The specimen tested under variable amplitude loading was a run-out at one million load cycles.

### 3.5 Fracture surfaces

On the basis of the fracture surface analysis, three different fatigue crack initiation types are observed: rolled plate surface, plate corner, and plasma-cut edge. Figure 11 presents an example of each location of the fatigue crack initiation, while Table 7 summarizes the crack initiation locations for all the test specimens. In the case of 690 grinded, 690 grinded and sandblasted, and 355 grinded and sandblasted specimens, the crack initiated mostly from the corner or the plate surface. For 355 grinded specimens, the crack initiated only from the plate surface. In the case of 690 grinded series, also subsurface crack initiation was encountered in two specimens with inclusion size up to 100  $\mu\text{m}$  (see Figs. 12 and 13). In these cases, however, reduction of fatigue strength due to inclusion was not observed; see the

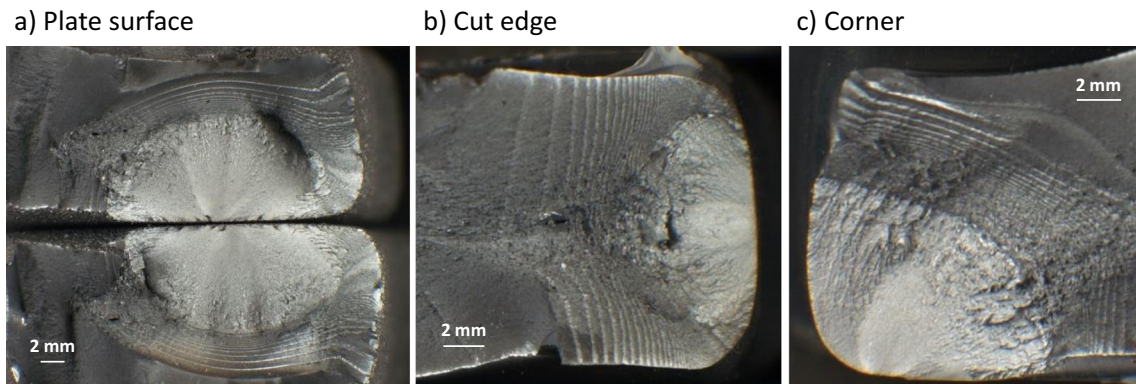
**Fig. 10** Fatigue test results



**Table 6** Summary of constant amplitude fatigue test results (retested run-out specimens excluded from the statistical analysis) and comparison to previous results from the literature

Test series	Plate thickness (mm)	Total no of specimens (run-outs)	Stress ratio R (-)	FAT class $P_s = 97.7\%$ (MPa)	Slope m (-)	Scatter 1:T $\sigma$ (-)
690 grinded <sup>a</sup>	15	11 (2)	0.1	501	15.4 <sup>a</sup>	1:1.26
690 grinded and sandblasted	15	14 (1)	0.1	562	15.4	1:1.07
355 grinded <sup>a</sup>	17	4 (1)	0.1	345	15.4 <sup>a</sup>	1:1.04
355 grinded and sandblasted <sup>a</sup>	17	10 (1)	0.1	312	15.4 <sup>a</sup>	1:1.16
690 grinded [5]	15	8 (0)	0.1	603	34.7	1:1.07
690 grinded and sandblasted [5]	15	7 (1)	0.1	591	52.0	1:1.03
355 grinded [5]	17	4 (1)	0.1	282	7.1	1:1.01
690 plasma cut, untreated [5]	15	10 (2)	0.1	268	4.1	1:1.25
700 plasma cut [23]	16	12 (3)	0.1	202	3.66	
700 plasma cut [22]	5	11 (2)	0.1	325	5	
355 plasma cut [22]	15	10 (3)	0.1	236	5	
700 plasma cut [8]	6–12		0.1	250	5	

<sup>a</sup> The slope of the fitted curve is flat or even rising with the number of cycles; thus, the definition of S-N curve properties is not possible and fixed slope value is used

**Fig. 11** Examples of fracture surfaces with initiations from plate surface (a), cut edge (b), and corner (c)

black circle in Fig. 10. Figure 14 shows the corner crack initiation for 690 grinded specimens that had the

lowest fatigue strength. The fracture surface indicates possible material defects very close to the surface.

**Table 7** Summary of crack initiation locations

Series	Initiation location			
	Plate surface	Cut edge	Corner	Subsurface
690 grinded	1	1	7	2
690 grinded and sandblasted	4	2	8	0
355 grinded	4	0	0	0
355 grinded and sandblasted	5	1	4	0

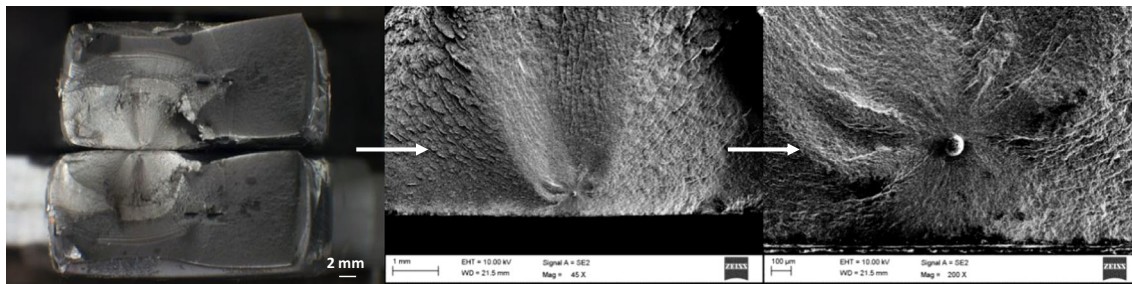


**Fig. 12** Subsurface crack initiation of NV-G-4

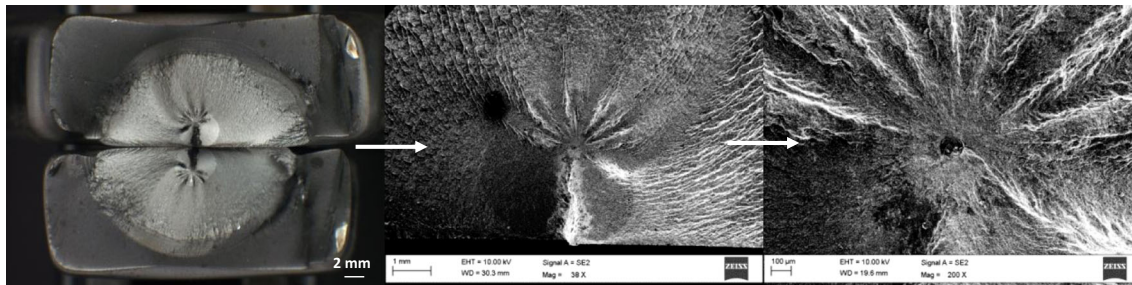


**Fig. 13** Subsurface crack initiation of NV-G-3\*

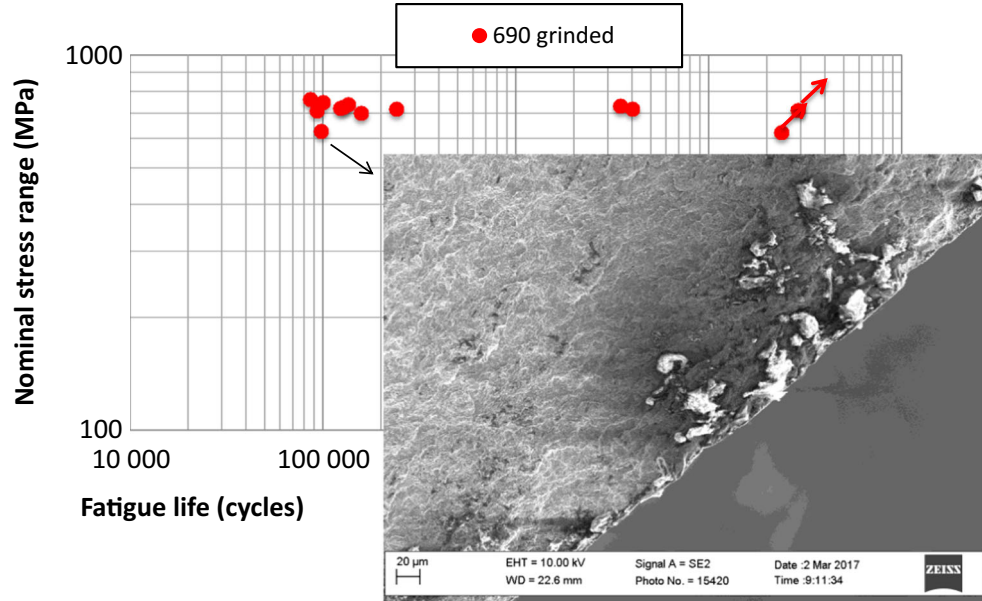
## 4 Discussion

Plasma cut high-strength steel post-cut treated in the shipyard production environment show significantly increased fatigue strength compared to the design curve FAT160 [3]. 690 steel has much higher fatigue strength than 355, but the difference

between only grinded or grinded and sandblasted specimens is small. Compared to untreated plasma cut edges, the improvement is up to 100% for 690 and about 30–40% for 355 steel (see Table 6).

The fatigue strength is high, but the slopes of the test data are quite flat or even rising with the number of

**Fig. 14** Crack initiation location for the specimen with the lowest fatigue strength



cycles and the definition of statistical parameters of the S-N curve is therefore not possible. In addition, large scatter in the results is observed for 690 grinded specimens. Flat slope and scatter in the results are related with three factors. First is the variation in the surface roughness. Surface roughness height is significantly smaller in grinded surfaces, but the peaks and valleys are also sharper and could have acted as initial cracks. This results in higher sensitivity of grinded surfaces to final surface quality. Furthermore, these results highlight that the surface quality and the related fatigue strength cannot be expressed just by the height of the roughness as done in current standards and rules (see, e.g., [21, 24]). In addition, the shape of the roughness profile should be considered.

The second reason for flat slope and scatter is related with the material internal quality. For example, large inclusions even up to  $100 \mu\text{m}$  in size were observed, but they did not decrease the fatigue strength unlike that reported for small-scale laboratory specimens in, e.g., [25, 26] and [27]. On the other hand, defects very close to surface may have influenced the fatigue strength of the specimen with the lowest fatigue strength (see Fig. 14).

The third source of flat slope and scatter is the variation in residual stress. A large scatter between and within specimens was observed (see Fig. 9). Considering the results of plasma cut untreated surfaces in [5, 23], the compressive residual stress seems to be caused by grinding. After sandblasting, the compressive residual stresses relaxed in the plate surface but not in the hardened cut edge. The whole production process of plasma cutting, grinding, and sandblasting influences the hardened layer, the residual stress states, and the surface quality (see, e.g., [28–31]). Therefore, the influence of different production parameters should be further studied and optimized. Furthermore, the post-cut treatment of corners should receive extra attention as more than half of the specimens in this study failed from there.

The results presented in this and previous studies, [5, 8, 22, 23], were obtained under constant amplitude loading with the stress ratio of  $R=0.1$ . However, realistic loading of cruise ships includes variable amplitudes with over- and under-loads. In addition, higher mean stresses could occur in some parts of the structure due to still water bending moment. It is very important to check the fatigue resistance under realistic loading, especially because part of the fatigue strength increase can be attributed to the compressive residual stresses. Overloads may relax these beneficial residual stresses and reduce the fatigue strength. This study included just

one 690 grinded and sandblasted specimen tested under WASH spectrum loading with the maximum stress close to yield limit and  $R=0.5$ . No failure was encountered within one million load cycles, but more systematic investigation is required.

In addition, utilization of high-strength steels in large marine applications requires a holistic design approach as high fatigue strength in cut edges may shift the critical location to the next weakest link, for example, to the closest weld.

## 5 Conclusions

This paper investigated the fatigue strength of high-strength steel that had gone through the shipyard production process of plasma cutting, grinding, and sandblasting. Based on the results of constant amplitude loading tests at the stress ratio of  $R=0.1$ , the following conclusions can be drawn:

- Fatigue strength of plasma-cut surfaces can be significantly improved with the post-cutting treatment applicable for shipyard production environment. The increase is achieved through introducing compressive residual stress and reducing the surface roughness height using grinding.
- 690 steel has significantly higher fatigue strength compared to 355 steel, but the difference between grinded or grinded and sandblasted surfaces is small, even though the difference in surface roughness height is about 10 times. The fatigue strength after sandblasting did not drop significantly thanks to smoother surface roughness shapes.
- Flat slopes of S-N curves and scatter in the results are associated with the variations in the surface roughness, material quality, and residual stress.
- Inclusions even up to  $100 \mu\text{m}$  in size did not decrease the fatigue strength.

Further experiments under realistic loading are required to understand the influence of residual stresses and over- and under-loads as well as high mean stresses on the fatigue strength.

## Appendix

Fatigue test results are given in Table 8. The “+” sign indicates multiple crack initiation sites, and “\*” indicates retested run-out specimen.

**Table 8** Fatigue test results

Test specimen (index)	Dimensions		Load ratio (-)	Nominal stress range (MPa)	Fatigue life (cycles)	Failure location
	Thickness (mm)	Width (mm)				
690 grinded R = 0.1						
NV-G-1	14.9	30.8	0.1	700	157,968	Corner
NV-G-2	14.7	30.8	0.1	627	97,799	Corner
NV-G-3	14.9	31.1	0.1	622	23,800,000	Run-out
NV-G-3*			0.1	719	4,019,754	Subsurface
NV-G-4	14.7	31.2	0.1	731	3,477,989	Subsurface
NV-G-5	14.7	31.1	0.1	763	86,094	Rolled surface
NV-G-6	14.8	31.1	0.1	738	135,393	Corner
NV-G-7	14.8	30.9	0.1	713	28,986,058	Run-out
NV-G-7*			0.1	748	100,250	Cut edge+
NV-G-8	14.8	31.2	0.1	727	127,825	Corner
NV-G-9	14.8	31.1	0.1	722	123,246	Corner
NV-G-11	14.7	30.9	0.1	718	240,812	Corner
NV-G-12	14.7	31.0	0.1	711	93,250	Corner
690 grinded and sandblasted R = 0.1						
NV-GS-1	14.9	31.1	0.1	706	244,871	Corner
NV-GS-2	14.8	30.9	0.1	694	185,942	Cut edge
NV-GS-3	14.9	31.2	0.1	978	190,094	Corner
NV-GS-4	14.8	30.9	0.1	681	256,225	Cut edge
NV-GS-5	14.9	31.0	0.1	679	247,947	Corner
NV-GS-6	14.9	31.1	0.1	675	286,783	Rolled surface
NV-GS-7	14.9	31.2	0.1	670	395,925	Corner
NV-GS-8	14.9	31.0	0.1	669	419,777	Rolled surface
NV-GS-10	14.9	31.1	0.1	657	360,997	Rolled surface
NV-GS-11	14.8	31.1	0.1	640	347,546	Corner
NV-GS-12	14.8	31.2	0.1	620	478,799	Corner
NV-GS-13	14.9	30.9	0.1	607	2,052,492	Rolled surface
NV-GS-14	14.9	31.1	0.1	599	1,126,594	Corner
NV-GS-15	14.8	31.0	0.1	593	26,800,000	Run-out
NV-GS-15*			0.1	632	303,936	Corner
690 grinded and sandblasted VAL						
NV-GS-9	14.9	31.2	0.5	$\sigma_{\max} = 812$	1,000,000	Run-out
355 grinded R = 0.1						
NS-G-3	17.2	29.5	0.1	414	266,870	Rolled surface
NS-G-4	17.4	31.0	0.1	415	157,723	Rolled surface
NS-G-5	17.1	29.9	0.1	403	20,500,000	Run-out
NS-G-5*			0.1	422	404,896	Rolled surface
NS-G-6	17.3	30.9	0.1	413	190,503	Rolled surface
355 grinded and sandblasted R = 0.1						
NS-GS-1	17.2	30.0	0.1	409	142,065	Cut edge+
NS-GS-2	17.2	29.9	0.1	398	341,091	Rolled surface
NS-GS-3	17.3	29.7	0.1	391	8,547,926	Rolled surface
NS-GS-4	17.1	30.5	0.1	395	669,964	Rolled surface
NS-GS-5	17.4	31.3	0.1	380	23,729,388	Run-out
NS-GS-5*			0.1	395	283,938	Rolled surface
NS-GS-6	17.4	31.2	0.1	396	315,077	Rolled surface
NS-GS-7	17.2	29.7	0.1	397	264,009	Corner +
NS-GS-8	17.1	31.3	0.1	383	722,071	Corner
NS-GS-9	17.3	29.8	0.1	393	219,966	Corner
NS-GS-10	17.2	29.8	0.1	384	425,265	Corner +

## References

1. DNV GL (2015a) DNVGL-RU-9111:2015–7, “rules for classification, part 3 hull, chapter 9 fatigue”. DNV GL, Oslo
2. DNV GL (2015b) Class guideline DNVGL-CG-0129: “fatigue assessment of ship structures”. DNV GL, Oslo
3. Hobbacher A (2009) Recommendations for fatigue design of welded joints and components, IIW doc. 1823–07, Welding Research Council Bulletin 520, New York

4. De Jesus AMP, Matos R, Fontoura BFC, Rebelo C, de Silva LS, Veljakovic M (2012) A comparison of the fatigue behavior between S355 and S690 steel grades. *J Constr Steel Res* 79:140–150
5. Remes H, Korhonen E, Lehto P, Romanoff J, Niemelä A, Hiltunen P, Kontkanen T (2013) Influence of surface integrity on the fatigue strength of high-strength steels. *J Constr Steel Res* 89:21–29
6. Polezhayeva H, Badger C (2009) Effect of plate thickness on fatigue strength of base material and butt welded specimens made from EH40 steel thick plates: phase I. Proceedings of the Nineteenth International Offshore and Polar Engineering Conference, Osaka, Japan
7. Sperle J-O (2008) Influence of parent metal strength on the fatigue strength of parent material with machined and thermally cut edges. *Welding in the World* 52:79–92
8. Laitinen R, Valkonen I, Kömi J (2013) Influence of the base material strength and edge preparation on the fatigue strength of the structures made by high and ultra-high strength steels. *Procedia Eng* 66:282–291
9. IACS No.34 Standard Wave Data (2001)
10. Bathias C (1999) There is no infinite fatigue life in metallic materials. *Fatigue Fract Engng Mater Struct* 22(1999):559–565
11. Bathias C, Drouillac L, Le François P (2001) How and why the fatigue S-N curve does not approach a horizontal asymptote. *Int J Fatigue* 23:S143–S151
12. Wang QY, Bathias C, Kawagoishi N, Chen Q (2002) Effect of inclusion on subsurface crack initiation and gigacycle fatigue strength. *Int J Fatigue* 24:1269–1274
13. Marines I, Bin X, Bathias C (2003) An understanding of very high cycle fatigue of metals. *Int J Fatigue* 25:1101–1107
14. Marines-Garcia I, Paris PC, Tada H, Bathias C (2007) Fatigue crack growth from small to long cracks in very-high-cycle fatigue with surface and internal “fish-eye” failures for ferritic-perlitic low carbon steel SAE 8620. *Mater Sci Eng A* 468-470:120–128
15. Huang Z, Wagner D, Bathias C, Paris PC (2010) Subsurface crack initiation and propagation mechanisms in gigacycle fatigue. *Acta Mater* 58:6046–6054
16. Li W, Deng H, Sun T, Zhenduo S, Zhang Z, Lu L, Sakai T (2015) Subsurface inclusion-induced crack nucleation and growth behaviors of high strength steels under very high cycle fatigue: characterization and microstructure-based modeling. *Mater Sci Eng A* 641: 10–20
17. EN ISO 4288:1996 (1997). Geometrical product specifications (GPS)—surface texture: profile method—rules and procedures for the assessment of surface texture
18. EN ISO 6507-1:2005 (2005) Metallic materials—Vickers hardness test—part 1: test method
19. EN ISO 15305:2008 (2008). Non-destructive testing—test method for residual stress analysis by X-ray diffraction
20. Pook LP, Dover WD (1989) Progress in the development of a Wave Action Standard History (WASH) for fatigue testing relevant to tubular structures in the North Sea. *Development of Fatigue Loading Spectra, ASTM STP 1006*, Watanabe, Eds., American Society for Testing and Materials, Philadelphia, pp. 99–120
21. EN ISO 9013:2017 (2017). Thermal cutting—classification of thermal cuts—geometrical product specification and quality tolerances
22. Lefebvre F, Lieurade HP, Huther I, Jubin L (2015) Proposal for fatigue classes applicable to thermal cutting, IIW document XIII-WG4–138-15, International Institute of Welding
23. Stenberg T, Lindgren E, Barsoum Z, Barmicho I (2016), Fatigue assessment of cut edges in high strength steel—influence of surface quality, *Engineering Failure Analysis*
24. DNV GL (2015). DNVGL-RP-C203: “Fatigue design of offshore steel structures”, Oslo
25. Lei Z, Hong Y, Xie J, Sun C, Zhao A (2012) Effects of inclusion size and location on very-high-cycle fatigue behavior for high strength steels. *Mater Sci Eng A* 558:234–241
26. Zhang JM, Li SX, Yang ZG, Li GY, Hui WJ, Weng YQ (2007) Influence of inclusion size on fatigue behavior of high strength steels in the gigacycle fatigue regime. *Int J Fatigue* 29:765–771
27. Sun C, Lei Z, Xie J, Hong Y (2013) Effects of inclusion size and stress ratio on fatigue strength for high-strength steels with fish-eye mode failure. *Int J Fatigue* 48:19–27
28. Sasahara H (2005) The effect on fatigue life of residual stress and surface hardness resulting from different cutting conditions of 0.45%C steel. *Int J Mach Tools Manuf* 45:131–136
29. Thomas DJ (2011) The influence of the laser and plasma traverse cutting speed process parameter on the cut-edge characteristics and durability of Yellow Goods vehicle applications. *J Manuf Process* 12:120–132
30. Tingaev AK, Gubaydulin RG, Ilin IA (2016) Study of the effect of thermal cutting on the microstructure and chemical composition of the edges of workpieces made of steel brands S345, S390, International Conference on Industrial Engineering, ICIE 2016. *Procedia Eng* 150:1783–1790
31. Bursi OS, D’Incau M, Zanon G, Raso S, Scardi P (2017) Laser and mechanical cutting effects on the cut-edge properties of steel 355N. *J Constr Steel Res* 133:181–191